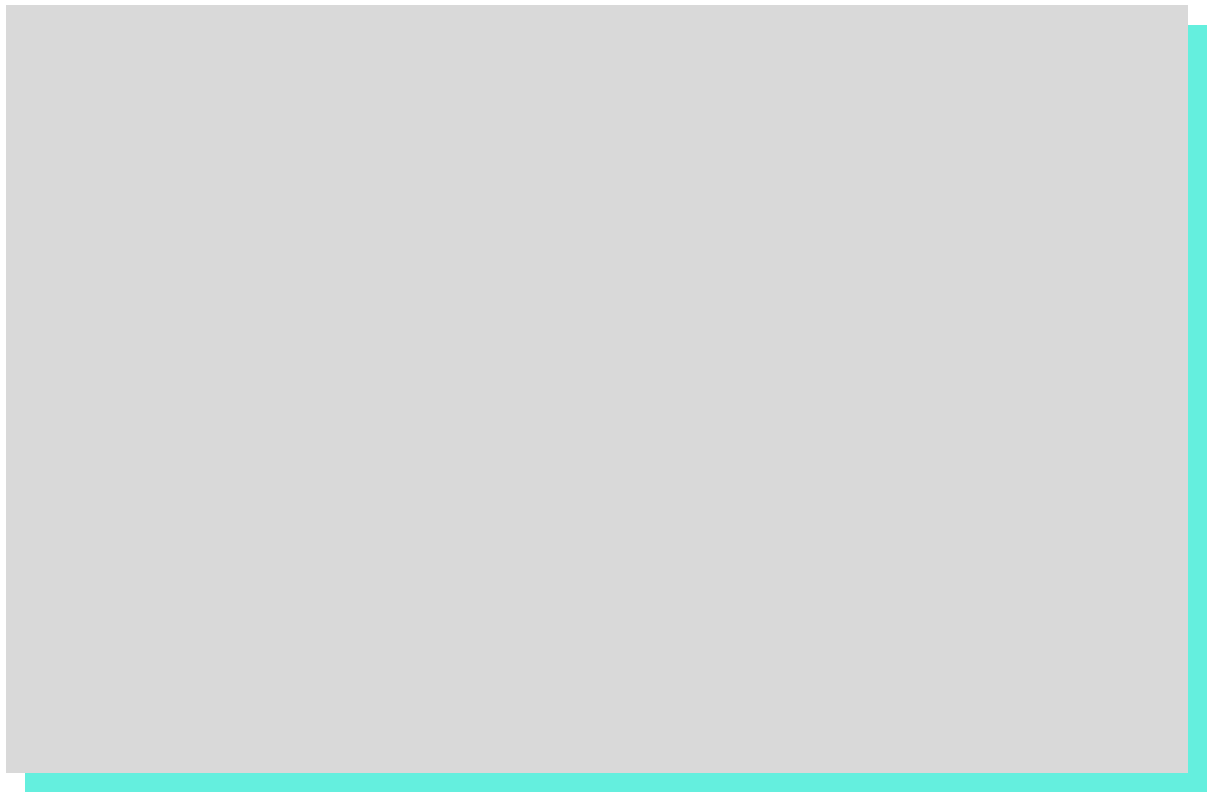**NORCE**

On the use of thermo-thickening polymers for in-depth mobility control

Core flood experiments at different scales

Arne Stavland, Daniel Strand and Siv Marie Åsen

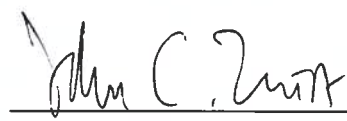|	
Project title:	On the use of thermo-thickening polymers for in-depth mobility control
	Core flood experiments at different scales
Project number:	100164
Institution:	NORCE
Client:	The National IOR Centre of Norway
Classification:	Confidential
Report no.:	6-2020

Stavanger, 24.02.2020

Arne Stavland
Project manager

Ingebret Fjelde
Quality assurance

John C. Zuta
Manager

1. Contents

Abstract

Here we confirm that low molecular weight ATBS-based associative polymers can be used for in-depth thermo-thickening.

To minimize the chemical degradation, at elevated temperature, the oxygen content was lowered by purging all fluids with N_2 gas. The base case polymer was the polymer A06, diluted to 1000 ppm, in synthetic seawater, SSW. This recipe did not show thermo-thickening at temperature up to 80°C and support previous finding from previously performed large scale tests. However, through systematic tests we confirmed that:

- Thermo-thickening is possible by increasing the A06 polymer concentration in SSW to 2700 ppm
- Thermo-thickening is possible at polymer concentration of 1000 ppm by increasing the associative content, i.e., using A08 or A10 polymers
- By increasing the brine salinity, from SSW to 3 times the SSW salinity thermo-thickening was more robust

We observed some thermo-thickening effect when increasing the core length from 7-cm to 76-cm using 1000 ppm A10 in SSW, but no length effect when the brine salinity was increased to 3 times SSW. It was concluded that thermo-thickening was not sensitive to type of porous media; flow behaviour in Berea and Bentheimer sandstones and high permeability sand pack experiments was similar.

To further up-scale the flood experiments, to multi-meter long columns, and to account for possible chemical degradation of the polymer, it is recommended to use a more robust system than the 1000 ppm A10 polymer in SSW. Here, we confirmed that increasing the brine salinity will help. From previous work it has also been confirmed that increasing the associative content, molecular weight and polymer concentration will work. When designing a new formulation, the following criteria should however be fulfilled, (i) No-thermo-thickening at low temperature (e.g., 20°C), (ii) Polymer concentration should not be unrealistically high and (iii) In terms of mechanical degradation, low molecular weight is preferred over high molecular weight polymers.

Therefore, increasing the associative content seems to be the preferred method.

1 Introduction

The EOR potential for polymers is through improved volumetric sweep efficiency. Associative polymers have the potential to outperform regular EOR polymer. The main reasons for this are the following:

- The improved sweep efficiency is dictated by the mobility ratio, that is $M = \lambda_w / \lambda_p$. The regular-polymer-viscosity depends on polymer concentration and Molecular weight, Mw, while associative polymers can form polymer networks which may significantly increase the apparent viscosity.
- Polymer viscosity is shear thinning, i.e., the viscosity increases by decreasing the shear rate. In porous media, the shear thinning for regular polymers is weak, while it may be significant for associative polymers.
- The mobility reduction for regular polymer is nearly insensitive to temperature, while for associative polymer, the mobility reduction may through thermo-thickening depend strongly on temperature.

These effects were illustrated in the following experiment, reported by Reichenbach-Klinke et al. (2017). An associative polymer was first flooded through a core at 20°C and the mobility reduction RF = 14.9 (lower right corner in Fig 1.1) corresponds to the relative polymer viscosity. Then, the temperature was increased to 60°C and the mobility reduction increased to RF = 152 (upper right corner). Thereafter the flow rate was lowered, and RF increased to RF = 562 (upper left corner). Finally, the temperature was lowered to 20°C and RF decreased to 15.9 (lower left corner).
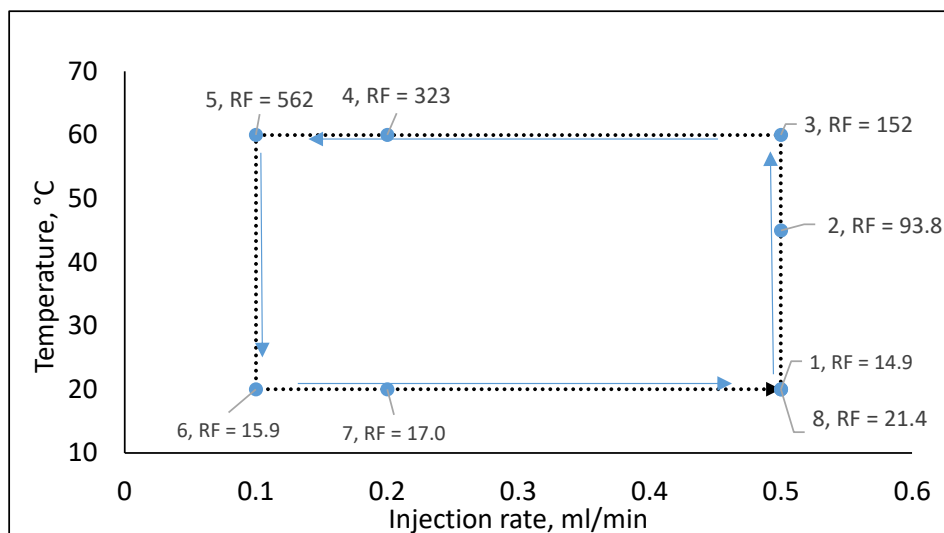

Fig. 1.1 Mobility reduction for 1000 ppm Aspiro^{TM} P6201 in SSW – Injection rate / Temperature sweep (from Reichenbach-Klinke et al. (2017).

The project objective is to demonstrate the potential for in-depth thermo-thickening. Two different types of flooding experiments were performed. Firstly, to mimic a temperature gradient, by injecting the polymer through multiple 7-cm cores with different temperatures, 20°C for the front core and 80°C for the outlet core. Secondly, the effect of core length was investigated in a 76-cm long sand column. Pressure ports along the length allowed for differential pressure reading across 4 sections of the column.

Parallel experiments have been performed by Halliburton in a 1-meter long column using the same type of polymer and sand with the possibility to vary the flow rate and temperature.

2 Theory

The mechanism for the high mobility reduction induced by the associative polymers is because of hydrophobic interactions between the polymer chains. The hydrophobic groups on the polymer backbone interacts with each other and form a polymer network. A sketch of such a polymer network is shown in Fig. 2.1.
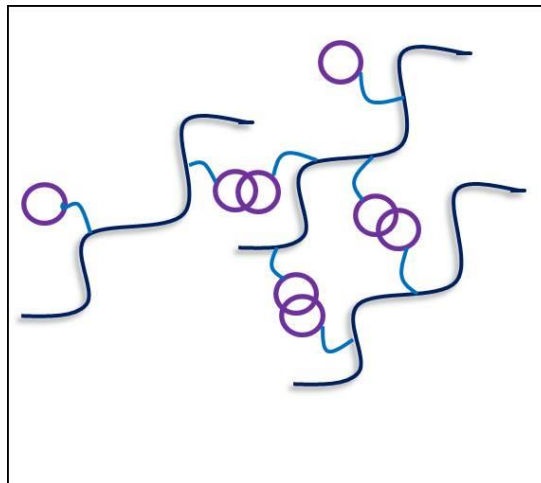

Fig. 2.1 Sketch of polymer network by associative polymers, from Lohne et al. (2019).

Experiments revealed that formation of polymer network is controlled by the concentration of hydrophobic groups, the molecular weight of the polymer, brine salinity and temperature. For a fixed associative polymer, both brine salinity and temperature (thermo-thickening) can be used to trigger the formation of the polymer network.

Lohne et al. (2019) presented a method to model the flow behaviour of associative polymer in porous medium. Their approach was that the associative polymer can be divided into two parts; the main part, pA with flow properties as a regular polymer and a smaller part, pB, with associative properties, i.e. the capability to form polymer network. Further, the retention of pB and increase in mobility reduction is independent of the polymer. The increased flow resistance by pB depends on the flow rate. By introducing Langmuir-type, retention models and permeability reduction derived from the Carman-Kozeny approach and linking the permeability to the specific surface area, Lohne et al. (2019) matched the experimental data.

3 Experimental methods

The polymers were low molecular weight ATBS-based associative polymers, delivered by BASF, and mixed in brine (SSW). Firstly, we prepared a mother solution at 10 000 ppm (1.0 wt%) which was further diluted by brine (SSW). The oxygen content was lowered by bubbling all fluids with nitrogen gas for at least 5 hours. Table 3.1 reports the ion composition for the SSW brine. Some experiments were performed in high salinity brine, i.e., 3XSSW.

Table 3.1 Brine compositions.

Salt	SSW	3XSSW
	g/liter	g/liter
NaCl	28.0	84.0
$CaCl_2$ x $2H_2O$	8.0	24.0
TDS	34.2	102.6

The flooding rig consisted of 3 serially mounted cores at temperatures of T1, T2 and T3, see Fig. 3.1. In addition, the setup contained 4 capillary tube viscometers (ID = 1.01 mm), one in front of first core at T1, one in front of second core at T2, one in front of the third core at T3 and the final one at the outlet of the third core at T3. Fluid was injected at constant rate using a Quizix pump and the differential pressures were measured with Fuji and Honeywell transmitters. A constant backpressure of 10 bar was applied.

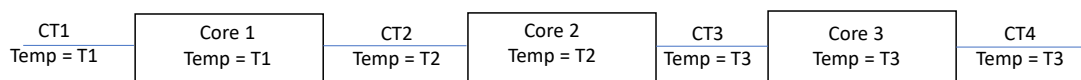| CT1	Core 1	CT2	Core 2	CT3	Core 3	CT4
Temp = T1	Temp = T1	Temp = T2	Temp = T2	Temp = T3	Temp = T3	Temp = T3

Fig. 3.1 Sketch of experimental set-up; flow through 3 serially mounted cores (C) and 4 capillary tube (CT) viscometers.

Mobility reductions were calculated from the ratio between polymer differential pressure and the brine baseline differential pressures.

4 Results core scale

Several experiments were performed, and the test conditions are summarized in Table 4.1. In these experiments the brine was SSW.

Table 4.1 Test conditions.

Exp.	Polymer	Conc.	Core type	T1	T2	T3
		ppm		°C	°C	°C
1a	A06-A35273	1000	Bentheimer	20	30	60
1b	A06-A35273	1000	Bentheimer	20	60	80
2	A06-A35273	2700	Bentheimer	20	60	80
3	A08-A33423	1000	Bentheimer	20	60	80
4	A10	1000	Bentheimer	20	60	80
5	A10	1000	Sand	20	60	80
6	A10-A40335	1000	Berea	20	60	80

As reported in Table 4.1, we have used two different batches of the A10 polymer. Brine viscosity vs. temperature is shown in Fig. 4.1. We assume that the polymer viscosity has the same temperature dependency as the makeup water, i.e. the relative viscosity, $\eta_r = \eta_p/\eta_w$, does not depend on temperature.

In this work we obtained the brine-baseline-mobilities at 20°C. Then, the mobility reduction was calculated as: $RF = \lambda_w/\lambda_p = \Delta P_p(T)/\Delta P_w(T = 20°C) \cdot \eta_w(T)/\eta_w(T = 20°C)$.

Here, λ is the mobility, ΔP is the differential pressure, η is the viscosity and T is the temperature. The indexes w and p are brine (water) and polymer, respectively.
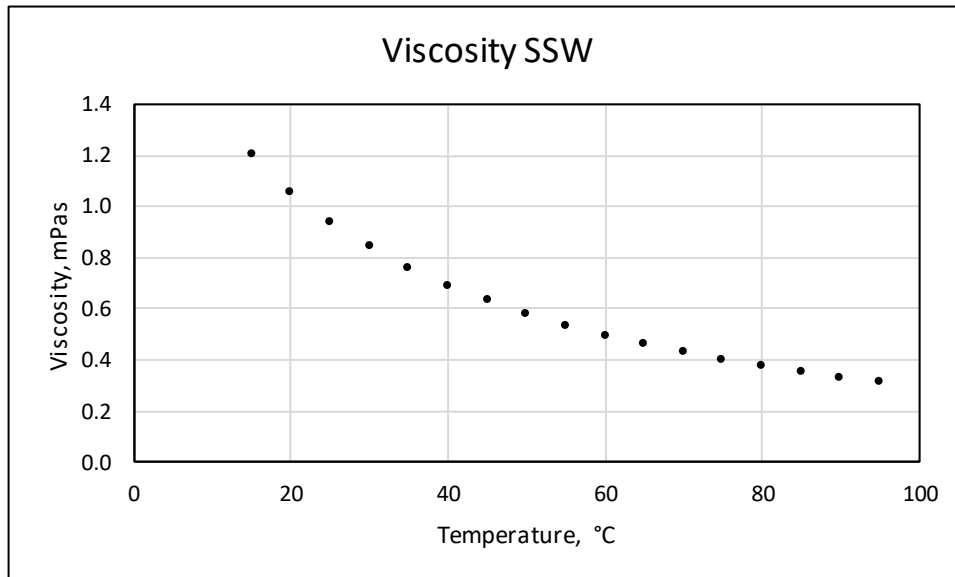
Fig. 4.1 Viscosity vs. temperature.

4.1 Bentheimer cores

Flood experiments 1 to 4 were performed in the same cores and the properties are given in Table 4.1.1.

Table 4.1.1 Bentheimer core properties.

	Core 1	Core 2	Core 3
Length, cm	6.98	6.97	6.94
Diameter, cm	3.78	3.78	3.78
Pore volume, mL	16.13	16.22	16.17
Porosity	0.207	0.208	0.208
Absolute permeability, Darcy	1.96	1.92	1.73

Fig. 4.1.1 shows the differential pressures across the cores and capillary tubes. The same data is in Fig. 4.1.2 plotted as mobility reduction. For convenience, the pore volume injected, pv, refers to the front core, C1.
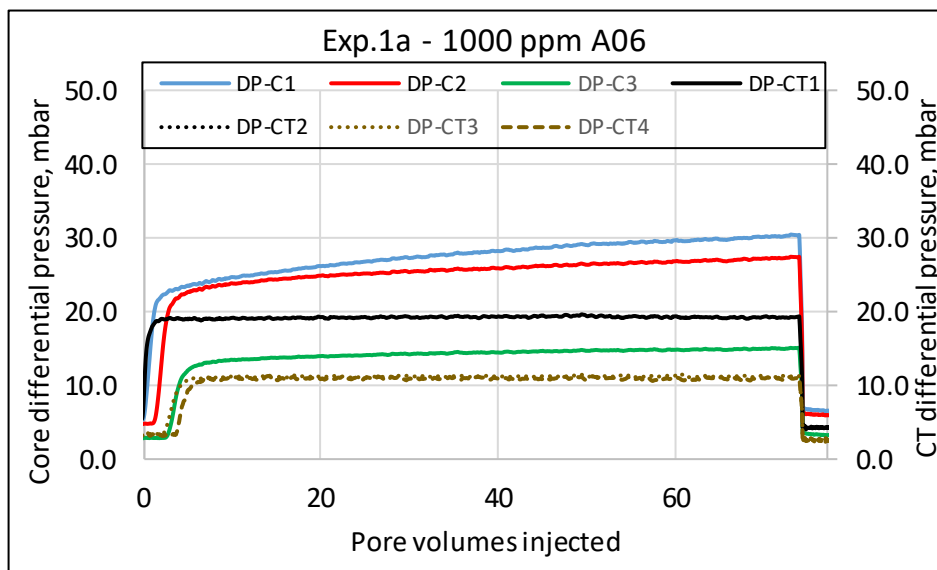
Fig. 4.1.1 Differential pressure (DP) across the Bentheimer cores and capillary tubes at T1 =20°C, T2 = 30°C and T3 = 60°C.
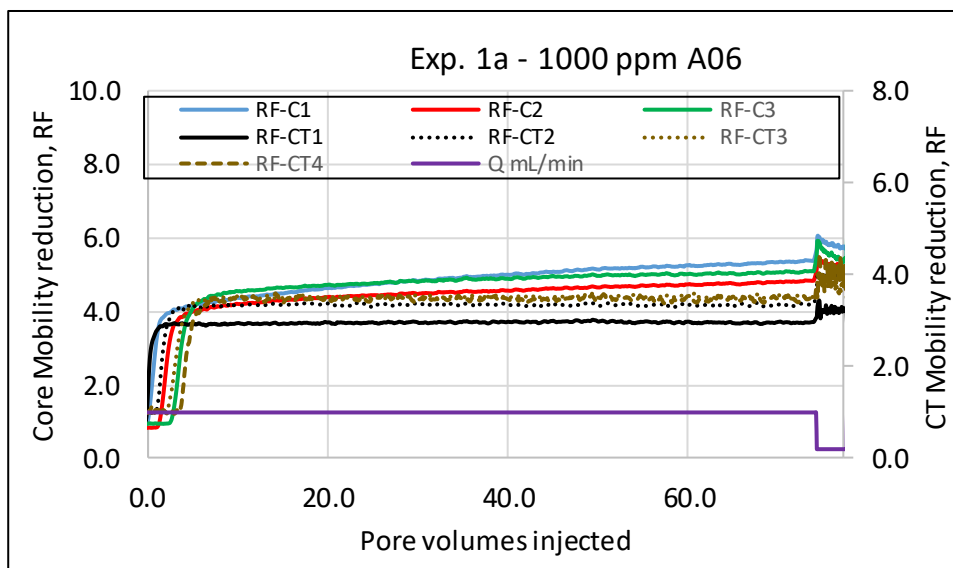

Fig. 4.1.2 Mobility reduction across the Bentheimer cores and capillary tubes at T1 =20°C, T2 = 30°C and T3 = 60°C.

Fig. 4.1.2 shows that core mobility reduction is independent of temperature and increases by decreasing the flow rate from q = 1.0 mL/min to 0.2 mL/min at pv = 74.3, i.e., the polymer has flow properties as a regular polymer.

Then, at pv = 77.6, the temperatures were shifted to T2 = 60°C and T3 = 80°C and the flow rate was increased to q = 1.0 mL/min. As seen in Fig. 4.1.3, there was no thermo-thickening effect for the combination 1000 ppm A06 in SSW at T = 80°C. Flow rate, in mL/min, is the plotted on the right vertical axis.
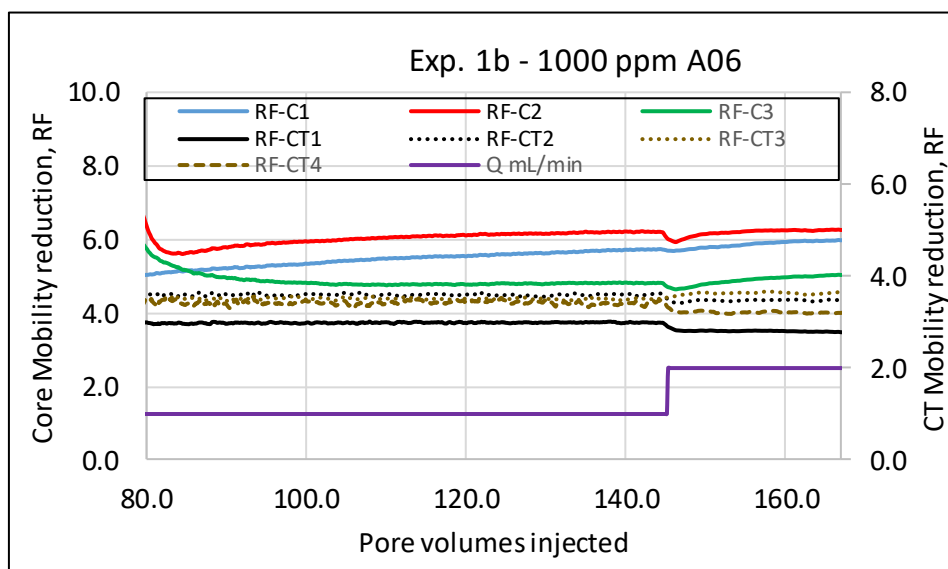
Fig. 4.1.3 Mobility reduction across the Bentheimer cores and capillary tubes at T1 =20°C, T2 = 60°C and T3 = 80°C.

We, therefore, at pv = 171.2, decided to increase the polymer concentration, from 1000 to 2700 ppm. Fig. 4.1.4 shows the evolution in mobility reductions. Note that core mobility reduction increased significantly by increasing the temperature, e.g. at q = 1.0 mL/min, RF-C1 = 19, RF-C2 = 41 and RF-C3 = 82. This effect is explained by thermo-thickening. When the flow rate was lowered to 0.5 mL/min (at pv = 270), RF-C2 and RF-C3 increased further.
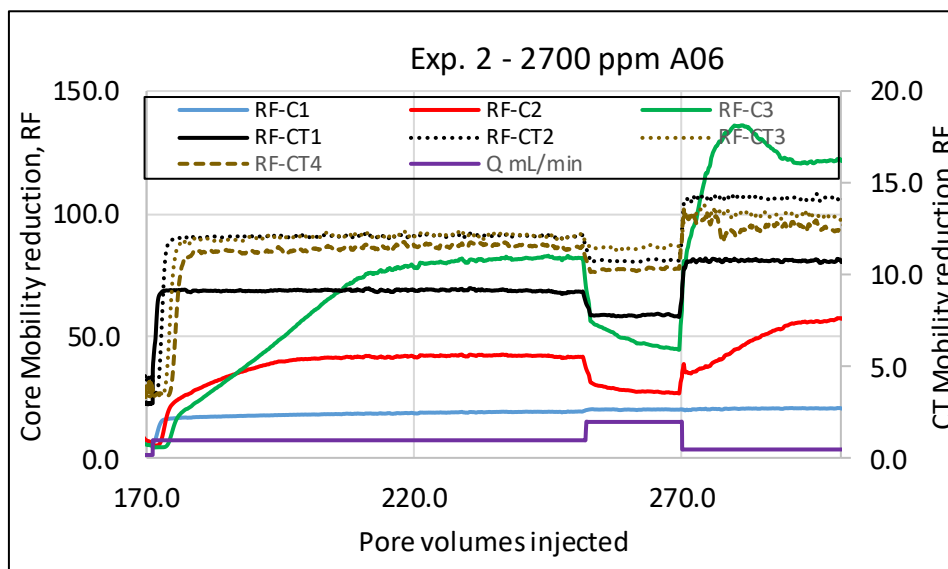

Fig. 4.1.4 Mobility reduction across the Bentheimer cores and capillary tubes at T1 =20°C, T2 = 60°C and T3 = 80°C.

However, when the flow rate was further reduced, to q = 0.2 mL/min, at pv = 302, we observed increased mobility reduction, followed by a collapse. Endpoint core mobility reductions at q = 0.2 mL/min were RF-C1 = 22, RF-C2 = 19, RF-C3 = 20. From Fig. 4.1.5, the capillary tube viscosity was stable, therefore the breakdown of the polymer network cannot be explained by polymer degradation.
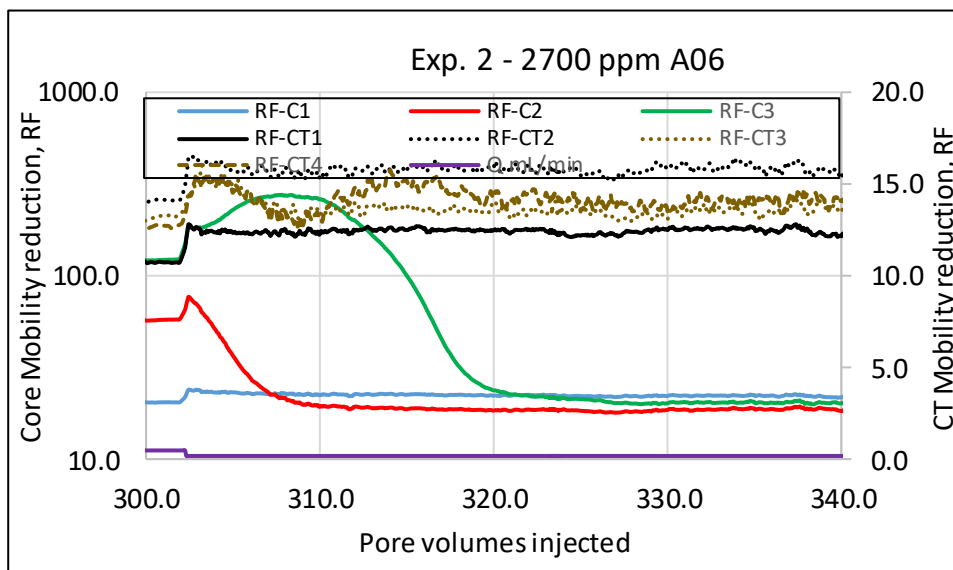
Fig. 4.1.5 Mobility reduction across the Bentheimer cores and capillary tubes at T1 =20°C, T2 = 60°C and T3 = 80°C.

To examine the effect of associative content, we continued the experiment by injection of the polymer A08. This polymer has higher associative content than the A06 polymer. As seen in Fig. 4.1.6, 1000 ppm A08 revealed thermo-thickening and stable core mobility reduction at q = 1.0 and q = 0.5 mL/min. At q = 0.2 mL/min (see Fig. 4.1.7), we observed breakdown of the polymer network, however, less dramatic than in the 2700 ppm A06 case.
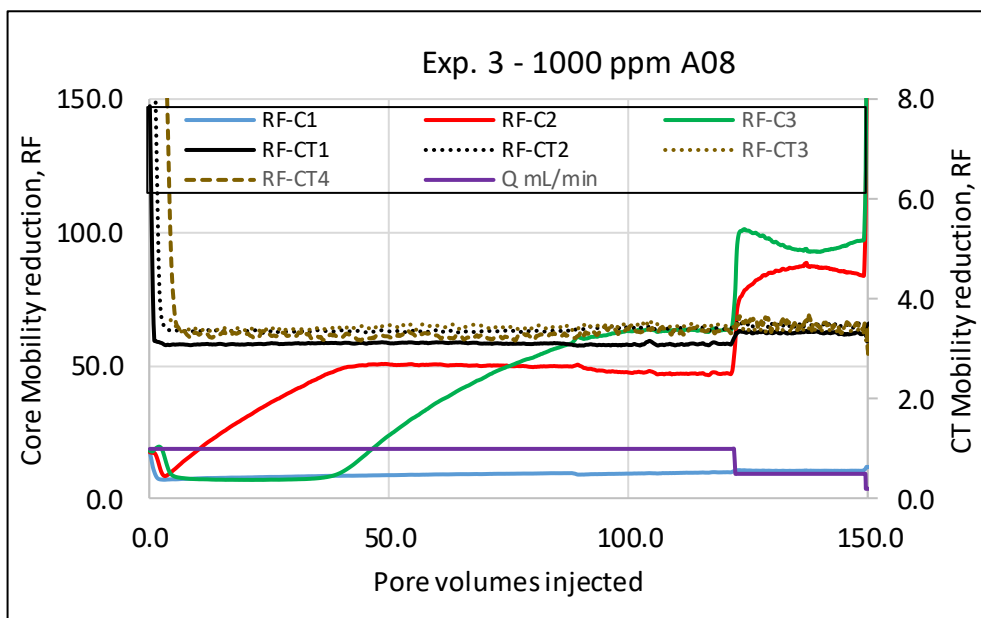

Fig. 4.1.6 Mobility reduction across the Bentheimer cores and capillary tubes at T1 =20°C, T2 = 60°C and T3 = 80°C.
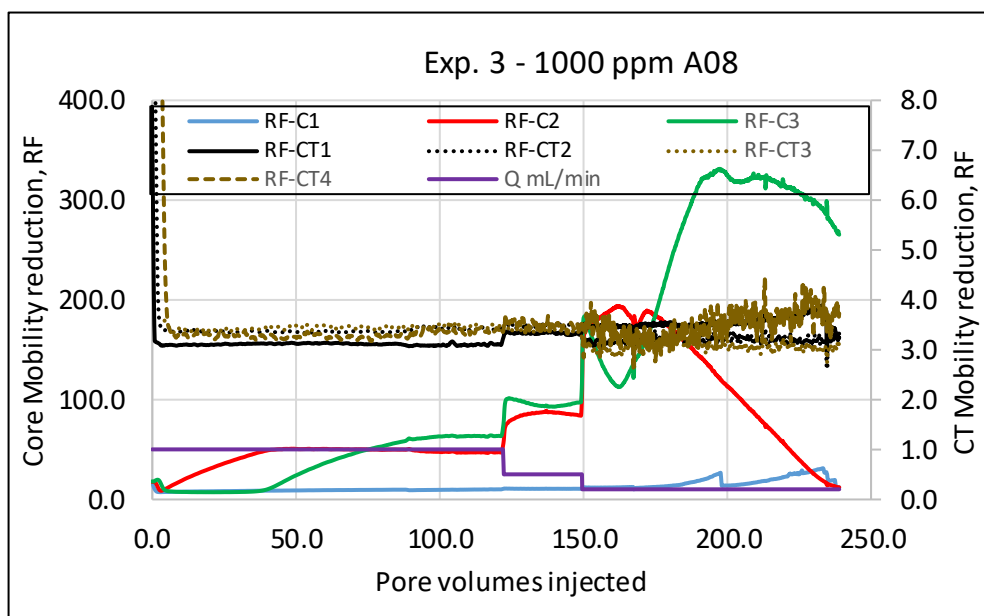
Fig. 4.1.7 Mobility reduction across the Bentheimer cores and capillary tubes at T1 =20°C, T2 = 60°C and T3 = 80°C.

Finally, we injected 1000 ppm of the A10 polymer. This polymer has higher associative content than the A08 polymer and we expected higher core mobility reduction at elevated temperature and improved stability at low injection rates, which is confirmed by the results shown in Fig. 4.1.8.
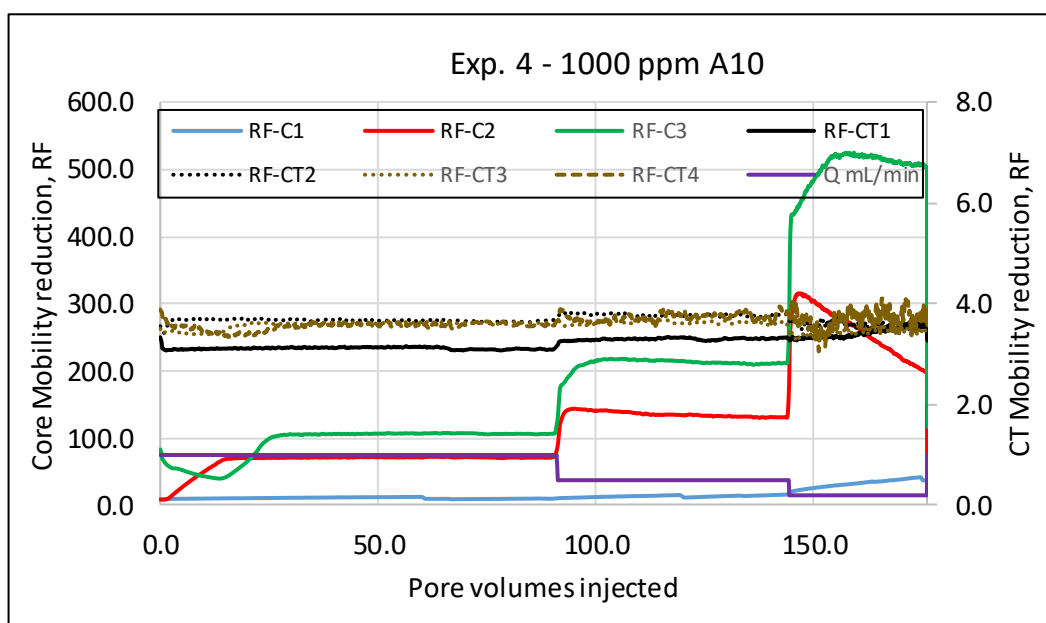

Fig. 4.1.8 Mobility reduction across the Bentheimer cores and capillary tubes at T1 =20°C, T2 = 60°C and T3 = 80°C.

Fig. 4.1.9 summarizes the Bentheimer core flood experiments. The black dotted lines are the relative polymer viscosity, measured on an Anton Paar rheometer. The mobility reduction derived from the capillary tubes is equal to the relative viscosity and is well

matched with the relative bulk viscosity. Here, the shear rate is derived from the Hagen-Poiseuille law, $\dot{\gamma} = 4v/r$. Similarly, for the core flood experiments $\dot{\gamma} = 4\alpha q/(A\sqrt{8k\varphi})$, where α is set to 2.5.

For the A06 polymer at 1000 ppm, the core mobility reductions are interpreted as insensitive of temperature. When the A06 polymer concentration was increased to 2700 ppm we observed thermo-thickening, i.e. RF increases by increasing the temperature and a more pronounced shear dependency. In Fig. 4.1.9, core mobility reduction at elevated temperature are plotted both as the maximum and endpoint values.

By increasing the associative content, from A6 to A08 or A10, we observed thermo-thickening even at polymer concentration of 1000 ppm. For the 1000 ppm A10 experiment, we observed shear dependent mobility reduction also at 20°C. It is however likely to assume that this is due to large throughput through the front core and not a thermo-thickening effect.
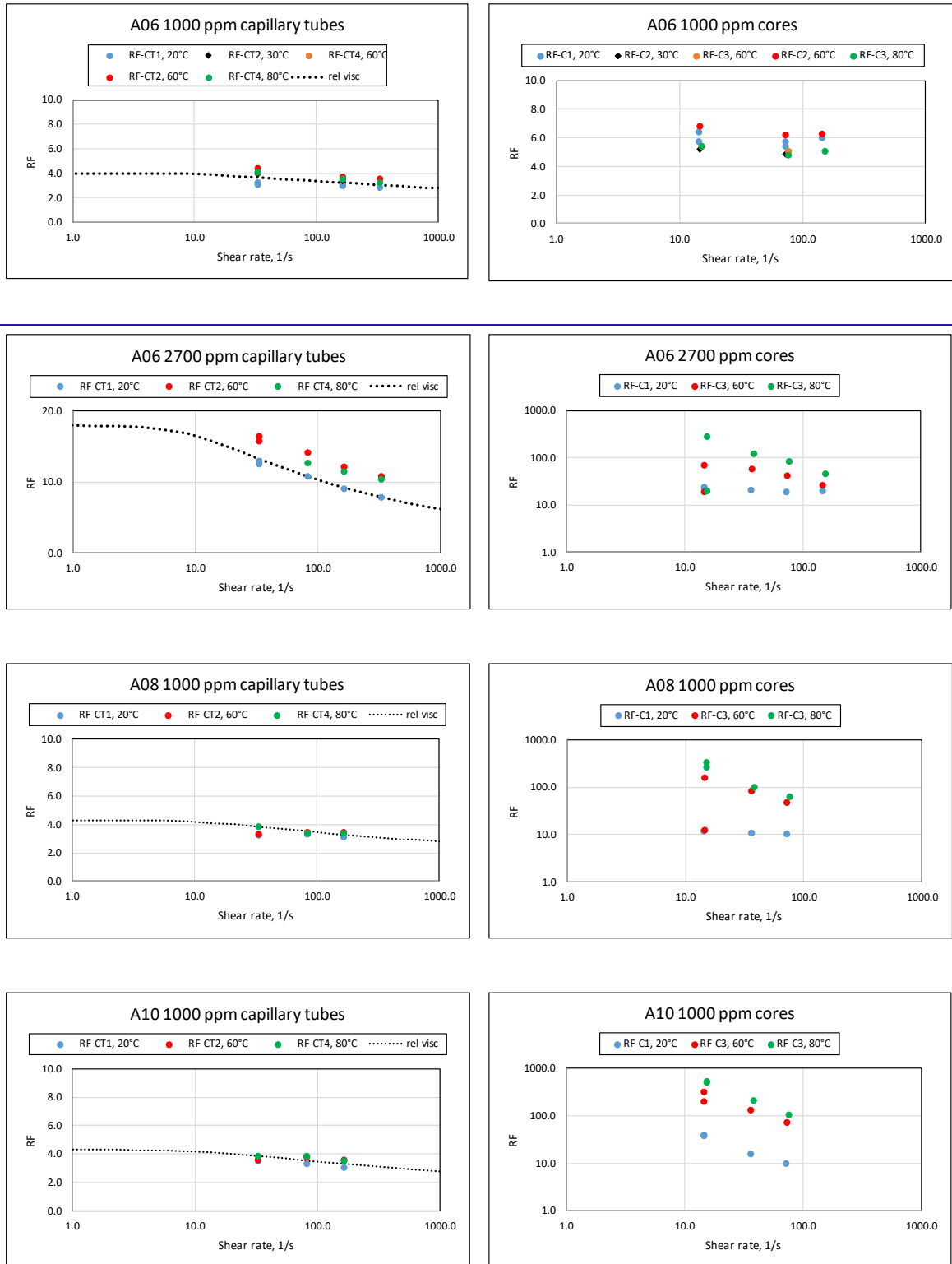
Fig. 4.1.9 Mobility reduction across the capillary tubes (left) and Bentheimer cores (right) at T1 = 20°C (blue), T2 = 60°C (red) and T3 = 80°C (green).

4.2 High permeability sand

The next experiment is a rerun of experiment 4, 1000 ppm A10, in 8 D quartz sand.

The sand was packed into core holders with overburden pressure of 50 bar. Thin slices (0.5 cm) of Bentheimer rock was used as screen, both at inlet and outlet. Table 4.2.1 shows the properties of the sand packs.

Table 4.2.1 Sand pack properties.

	Sandpack 1	Sandpack 2	Sandpack 3
Length, cm	8.85	8.39	8.06
Diameter, cm	3.79	3.78	3.78
Pore volume, mL	29.19	27.09	26.89
Porosity	0.293	0.288	0.297
Absolute permeability, Darcy	5.37	5.69	5.78
Sand permeability, Darcy	7.39	8.32	8.49

The absolute permeability is the permeability for the sand and screens combined. If the Bentheimer-slice permeability is 2 Darcy the effective sand permeability is, as reported in Table 4.2.1, approximately 8 Darcy. [Note that if we account for core compaction, i.e., the effective bulk volume is altered by the overburden pressure the sand permeability is increased by approximately 8%, see Appendix. The sand porosity was from the matrix-to-pore volume ratio calculated to 0.326.]

As in the Bentheimer case, Exp. 4, there is an effect of thermo-thickening. RF-C2 (at 60°C) is stable at flow rates of 1.0 and 0.5 mL/min. At these flow rate RF-C2 > RF-C3. This is probably because the flow rates were altered before equilibrium was reached at 80°C, see Fig. 4.2.1. As in Exp. 4 (injection of 1000 ppm A10 through Bentheimer cores) we experienced decline in RF-C2 at the lowest flow rate. However, when increasing the flow rate from q = 0.2 to q = 0.5 mL/min we observed pressure build-up. At equilibrium, the RF-C2 was the same as before.

Fig. 4.2.2 summarizes the flood experiment in high-permeability sand packs. The capillary tube relative viscosity matched the relative bulk viscosity while the thermo-thickening is observed in the sand.
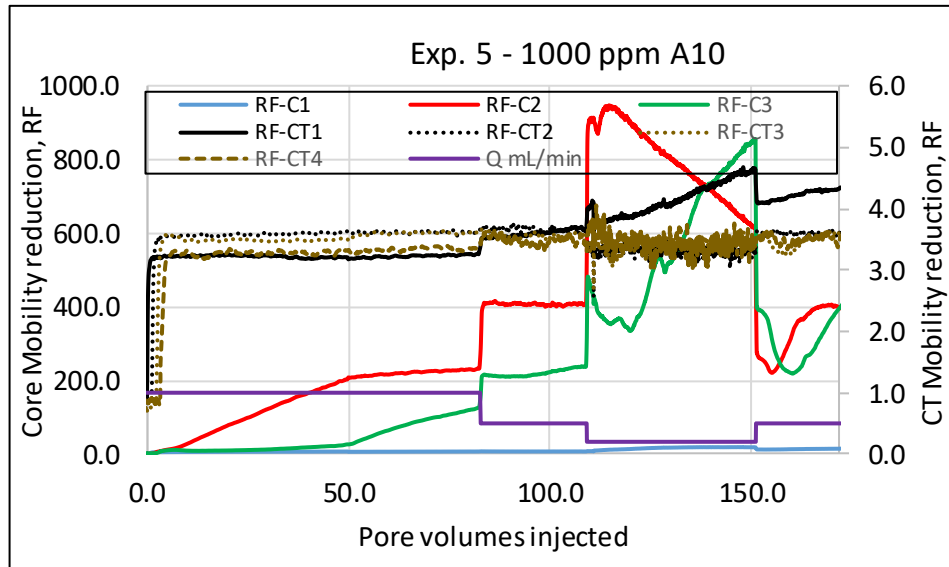

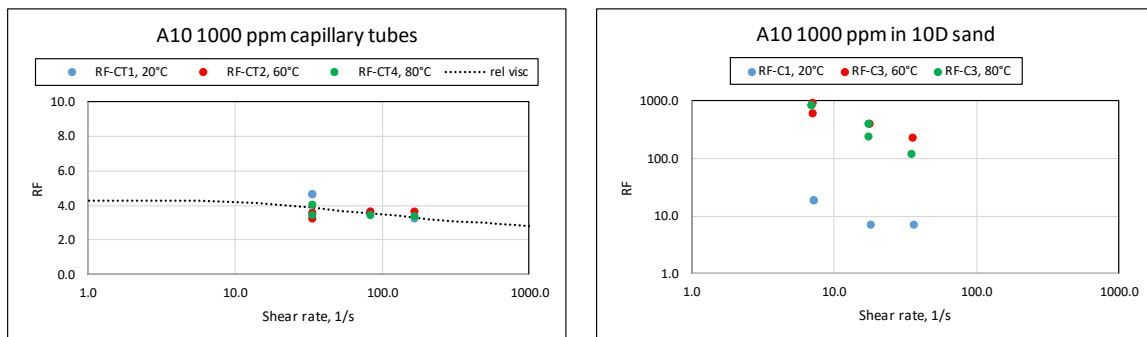Fig. 4.2.1 Mobility reduction across the sand packs and capillary tubes at T1 =20°C, T2 = 60°C and T3 = 80°C.

Fig. 4.2.2 Mobility reduction across the capillary tubes (left) and sand packs (right) at T1 =20°C (blue), T2 = 60°C (red) and T3 = 80°C (green).

4.3 Berea cores

The next experiment is a rerun of Exps. 4 and 5, 1000 ppm A10, in 0.7 Darcy Berea cores. Table 4.3.1 shows the properties of the Berea cores.

Table 4.3.1 Berea core properties.

	Core 1	Core 2	Core 3
Length, cm	7.04	7.06	7.05
Diameter, cm	3.78	3.76	3.76
Pore volume, mL	17.89	17.99	17.67
Porosity	0.226	0.229	0.226
Absolute permeability, Darcy	0.663	0.680	0.691

Porosity of Berea cores is slightly higher than the porosity of the Bentheimer cores. As in the previous A10-experiments, we also observed thermo-thickening in the Berea cores, see Fig. 4.3.1
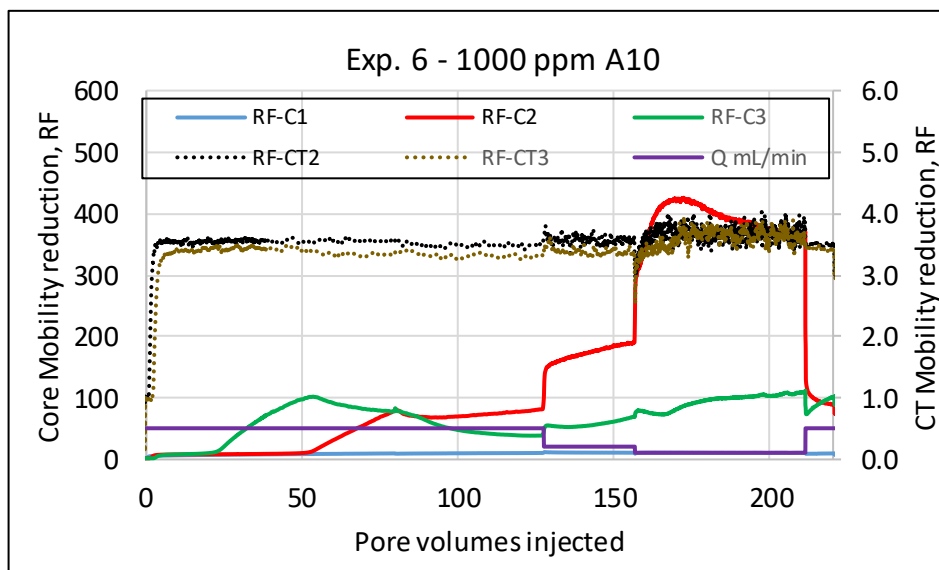

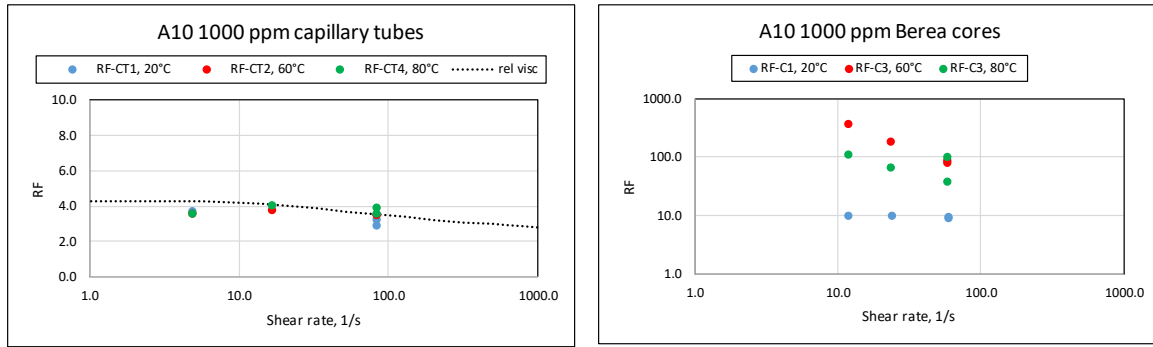Fig. 4.3.1 Mobility reduction across the Berea cores and capillary tubes at T1 =20°C, T2 = 60°C and T3 = 80°C.

Fig. 4.3.2 Mobility reduction across the capillary tubes (left) and Berea cores (right) at T1 =20°C (blue), T2 = 60°C (red) and T3 = 80°C (green).

Fig. 4.3.2 summarizes the Berea core flood experiment. Finally, Fig. 4.3.3 compares mobility reduction obtained in the 3 different types of porous media using the polymer 1000 ppm A10. As can be seen in Fig. 4.3.3, the associative polymer A10, is thermo-thickening at elevated temperature. At temperature of 20°C, the polymer behaves nearly as a regular polymer. Also note, the mobility reduction vs. shear rate is approximately the same for the three different types of porous media.
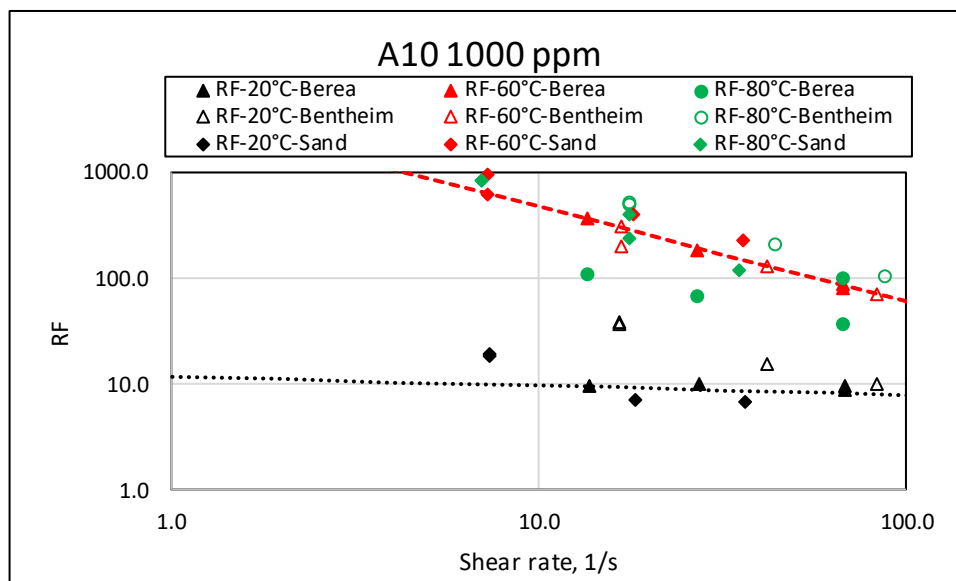

Fig. 4.3.3 Mobility reduction vs. shear rate for the three different porous media; 2D Bentheimer cores, 1D Berea cores and 8D quartz sand, at temperatures of 20, 60 and 80°C.

During post brine injection, we experienced a slow pressure decline, see Fig. 4.3.4. As an example, the permeability reduction in the Berea core at 80°C is more than 50, even after injection of 40 pvs of brine. For comparison, the pressure decline in the capillary type follows the saturation front.
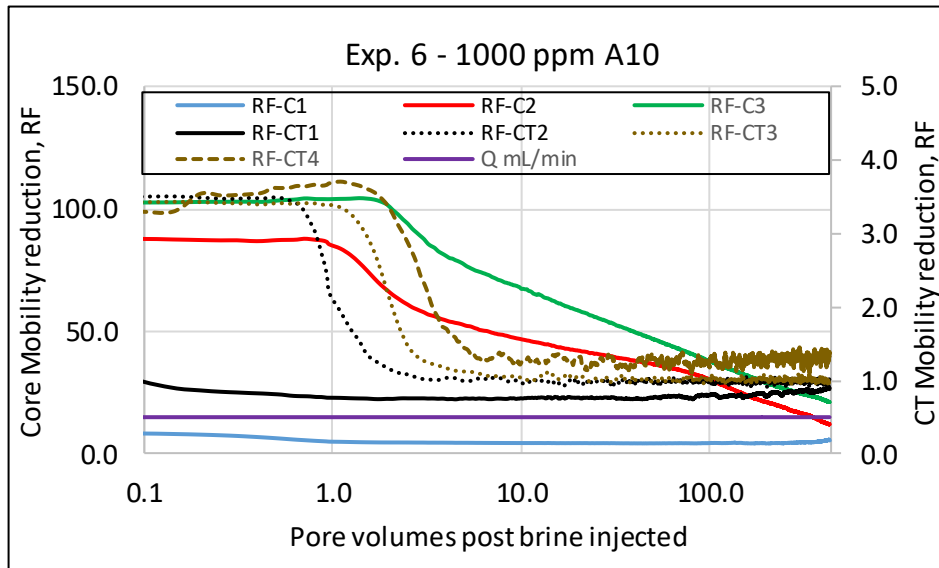
Fig. 4.3.4 Mobility reduction during post water injection in Berea cores.

For further optimization we should focus on associative polymers that show a more rapid pressure increase. At the conditions of SSW salinity and 1000 ppm of A10, the pressure start to increase after injection approximately 30 pv, see Fig. 4.3.1. It is likely that the thermo-thickening is more rapid if increasing the brine salinity, increasing the polymer concentration, Mw, or increasing the associative content. However, optimizing the product is assumed to be field specific and should therefore be addressed separately – in field specific studies.

5 Results large scale

In the next experiments we performed vertical flood experiment in a 76-cm long sand column with inner diameter of 5.36 cm. The temperature was here constant and differential pressure was measured across 4 equally long sections of columns.

The sand is the same as used in Exp. 5. It should be noted that effective sand permeability in Exp. 5 was 8 Darcy, while in Exp. 7 the permeability was 12 Darcy, see Table 5.1. This effect can be explained compaction of the sand using 50 bar overburden pressure in Exp. 5. It qualitatively agrees with Carmen-Kozeny:

$$k = \frac{\varphi^3 D_p^2}{72\tau(1-\varphi)^2}$$ Eq. 5.1

The particle size is constant, and we assume constant tortuosity, τ, then, $k = k(\varphi)$. The test conditions are summarized in Table 5.2.

Table 5.1 Sand pack properties.

	Total	Section 1	Section 2	Section 3	Section 4
Length, cm	**75.85**	18.96	18.96	18.96	18.96
Diameter, cm	**5.36**	5.36	5.36	5.36	5.36
Pore volume, mL	**592.34**	148.09	148.09	148.09	148.09
Porosity	**0.346**	0.346	0.346	0.346	0.346
Absolute permeability, Darcy	**11.78**	11.37	13.20	11.65	11.04

Table 5.2 Test conditions

Exp.	Polymer	Conc. ppm	Core	Brine	T °C
7	A10	1000	Sand	SSW	80
8	A10	1000	Sand	3XSSW	80
9	A10	1000	Sand	3XSSW	Temp-steps

The test conditions in Exp. 7 was like Exp. 5 but at constant temperature of 80°C and a new batch of the A10 polymer, A40602R. In terms of flow velocity, the injection rate of 3.0 mL/min, scaled to Exp. 5 conditions is equal to 1 mL/min. The polymer was injected through the pump, from a polymer reservoir. The reservoir was refilled daily, with 4 to 5 Liter of fresh polymer.
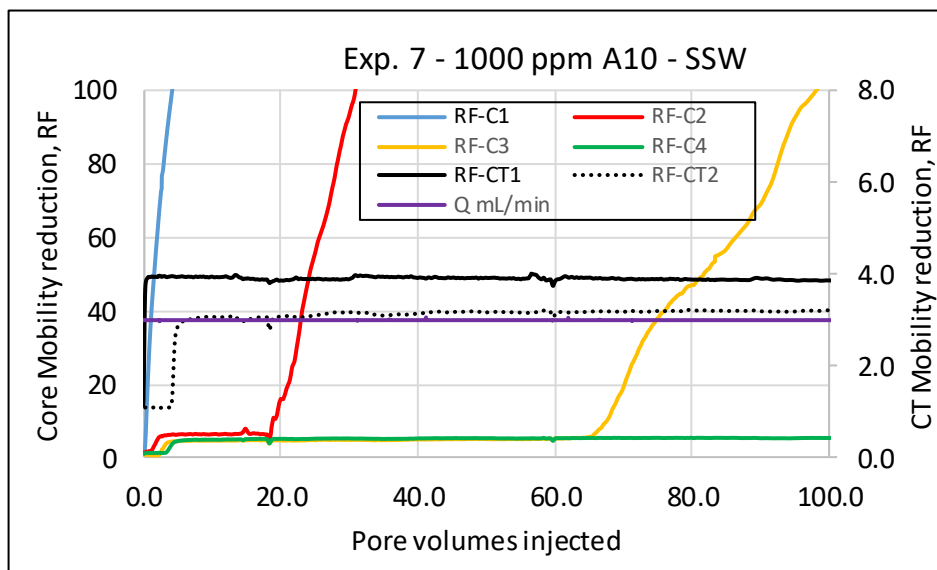
Fig. 5.1 Mobility reduction across the 4 sections of the 76-cm sand column at T =80°C.

Fig. 5.1 shows a rapid pressure increase in the 1st section, followed by pressure increase in 2nd section (after 19 pore volumes) and 3rd section (after 65 pore volumes). No thermo-thickening effect was observed in the 4th section, even though more than 260 pore volumes of polymer were injected, see Fig. 5.2. As for the previous experiments, pv refers to the pore volume of the first segment, i.e., equal to 148.09 mL.
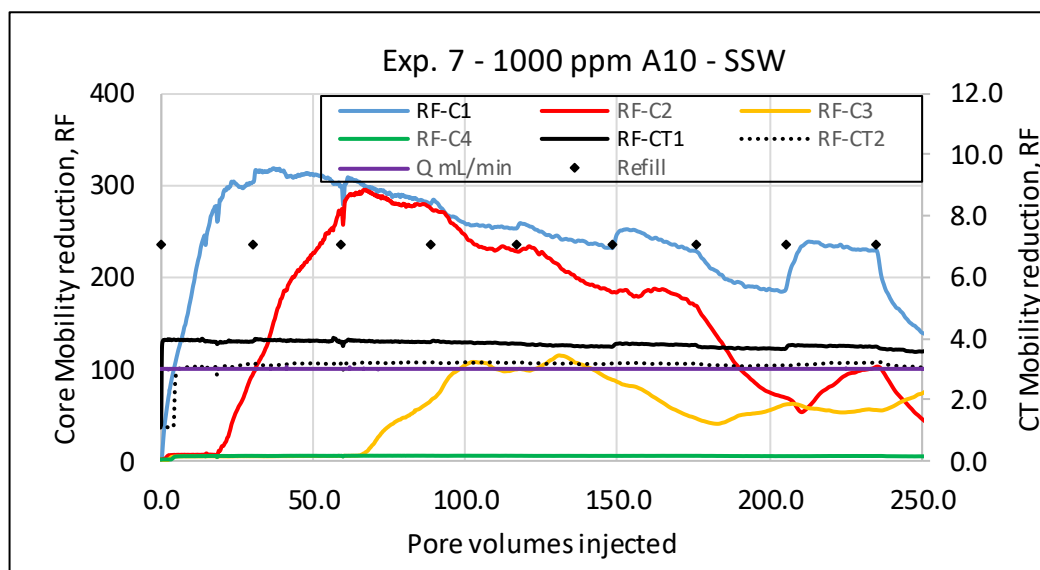

Fig. 5.2 Mobility reduction across the 4 sections of the 76-cm sand column at T =80°C.

Following observations were made:

- We observed some variation in polymer viscosity in the different 1000 ppm polymer samples, see Appendix 2. It is likely that this explains some of the RF(pv) variations. The black dots in Fig. 5.2 denotes when fresh polymer was added to the reservoir.
- The effluent viscosity seems to be lower than the injected (RF-CT2 < RF-CT1) and this may be due to degradation of the polymer. The residence time in the 76-cm sand

column at q = 3 ml/min is approximately 3.5 hours. (Compared with the previous 7-cm core flood experiments, the residence time of 3.5 hours corresponds to flow rates in 7-cm cores below 0.1 mL/min) A possible degradation of the polymer will thus reduce the thermo-thickening effect. By lowering the temperature (making the polymer more temperature stable) increasing the injection rate (lowering the residence time) increasing the polymer concentration or increasing the brine salinity are some of the options for more robust thermo-thickening.

- Thermo-thickening was observed in 3 out of 4 sections and highest RF was observed in the front section.

After injection of 262 porevolumes of 1000 ppm A10, in SSW, we increased the brine salinity in Exp. 8. 1000 ppm of the A10 polymer was prepared in brine with 3 times the salinity of SSW, 3XSSW. The mobility reduction during the 3XSSW polymer injection is shown in Fig. 5.3.
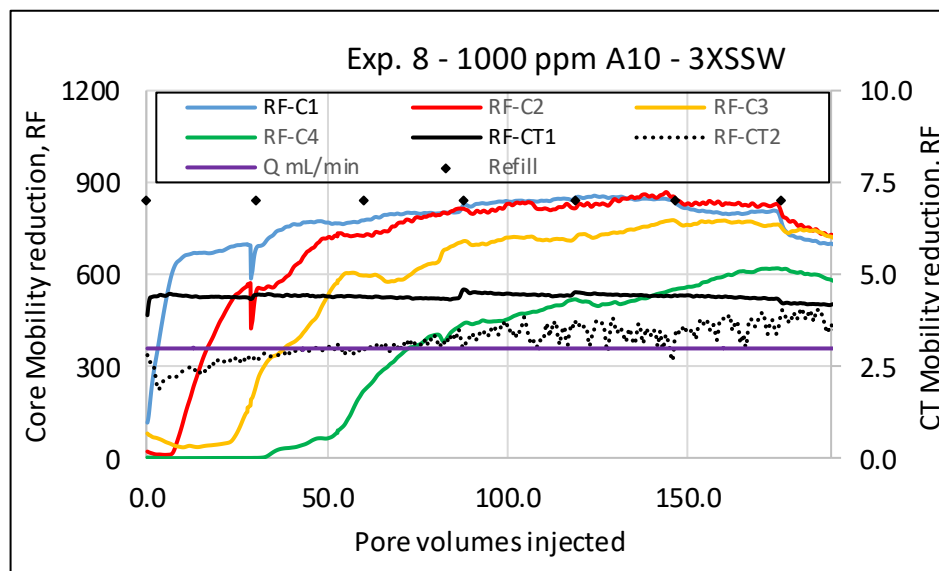

Fig. 5.3 Mobility reduction across the 4 sections of the 76-cm sand column at T =80°C.

As seen in Fig. 5.3, the A10 polymer at 1000 ppm, dissolved in 3XSSW, revealed thermo-thickening in all 4 sections. Fig. 5.4 shows an alternative method to represent the data, we plot $RFi = \frac{1}{i}\sum_1^i RFCi$ vs pore volume, i.e., RF3 is the mobility reduction across the first ¾ of the column with the corresponding pore volume of ¾ of the total pore volume. Assuming an ideal case, homogeneous permeability, no degradation of polymer and no length effect, the RFi's should overlap. Comparing Figs. 5.4 and 5.5, the experiment performed in 3XSSW is close to the ideal case. When using SSW, the deviation from the ideal case may be explained by degradation of polymer along the core length.
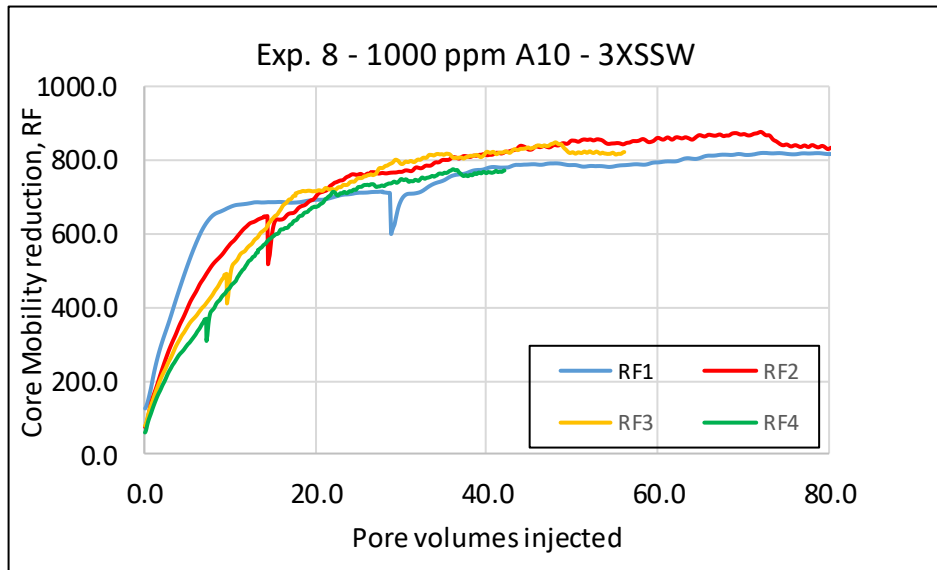
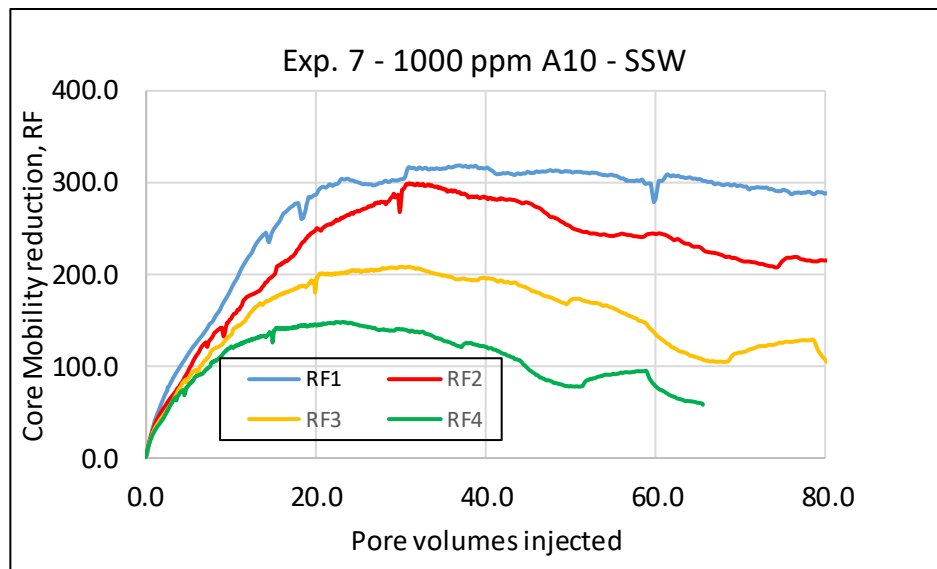Fig. 5.4 Mobility reduction vs. core length T =80°C.

Fig. 5.5 Mobility reduction vs. core length T =80°C.

After injection of 198 pv at q = 3 mL/min, the flow rate was lowered to q = 0.6 mL/min. Figs. 5.6 and 5.7 show that RF, in all sections, increased substantially by lowering the shear rate and $RF(\dot{\gamma})$ can, as reported above, be matched with a power-law dependency.
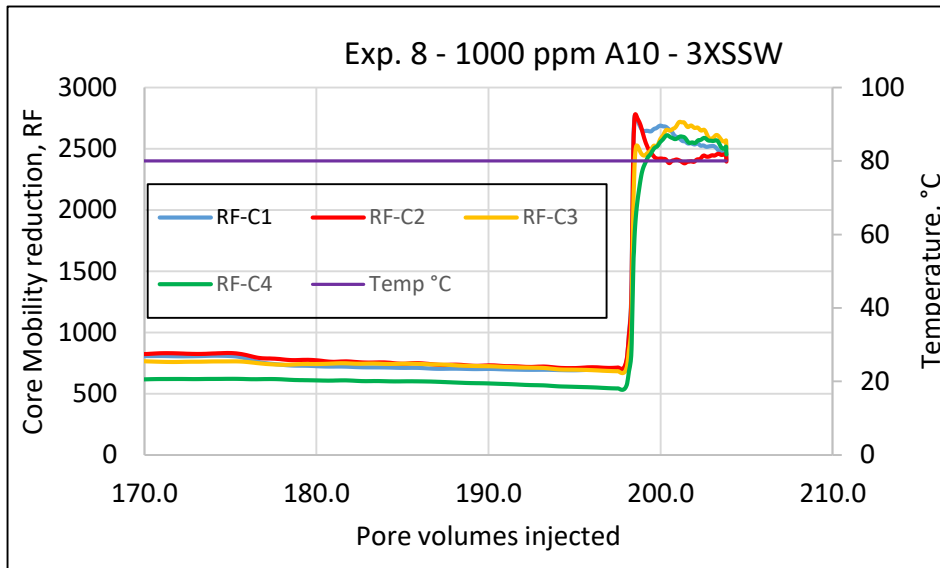
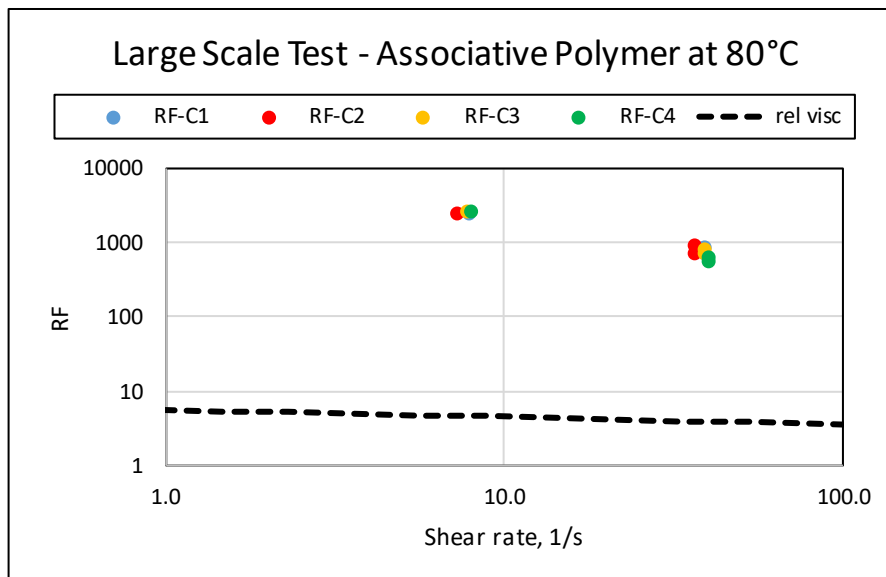Fig. 5.6 Mobility reduction at 80°C, flow rate lowered from q = 3.0 to q =0.6 mL/min at pv = 198.

Fig. 5.7 Endpoint core mobility reductions, 1000 ppm A10 in 3XSSW, vs. shear rate.

Then, fixing the flow rate to q = 0.6 mL/min, we performed temperature steps, see Figs. 5.8. Thermo-thickening is observed in all 4 sections at 60°C. At 40°C we report on slowly declining mobility reduction, first in the front section, then in the subsequent section, see Fig. 5.8. The RF-C1-decline at 40°C is expected to be because the temperature is below the critical on-set temperature for thermo-thickening. Why the process is slow and why the mobility reduction in subsequent core segments does not start before complete breakdown in previous segments are not fully understood. However, in previous work we have been able to match the RF-decline by a fluid train model. We assume that RF_0 is the mobility of regular polymer (no-thermo-thickening) and RF_A is the thermo-thickening mobility

reduction. For the relative front position, x, and x_A is a fraction, f, of x we can derive the effective RF in the following way:

$$RF = x_A RF_0 + (1 - x_A)RF_A$$ Eq. 5.2

By setting $f = 0.0077$ we were able to match both the RF-C1 and RF-C2 declines, see Fig. 5.9. From this approach we would expect decline also in RF-C3 and RF-C4. Instead of continuing the injection at 40°C and experimentally confirm the prediction of RF-decline, we decided to further lower the temperature to 20°C at pv = 438.
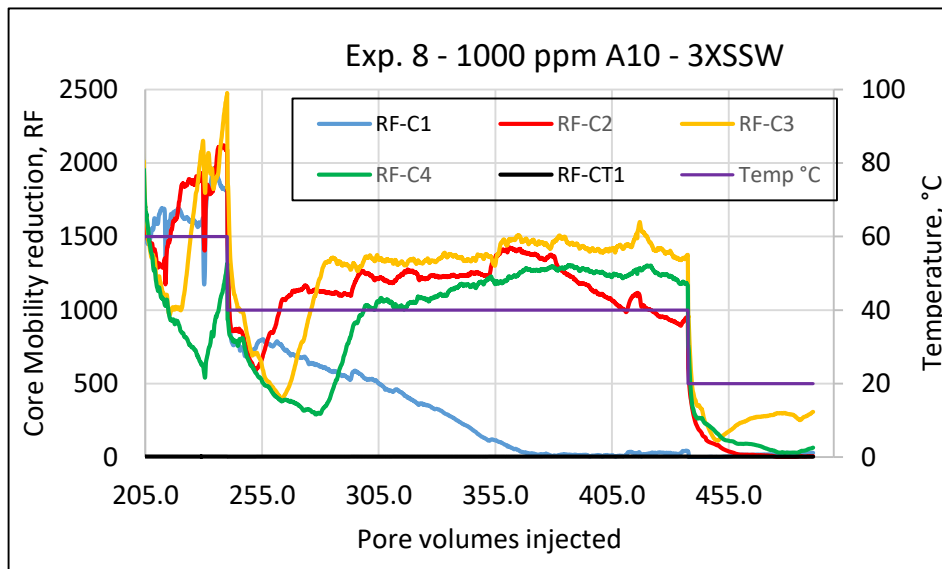

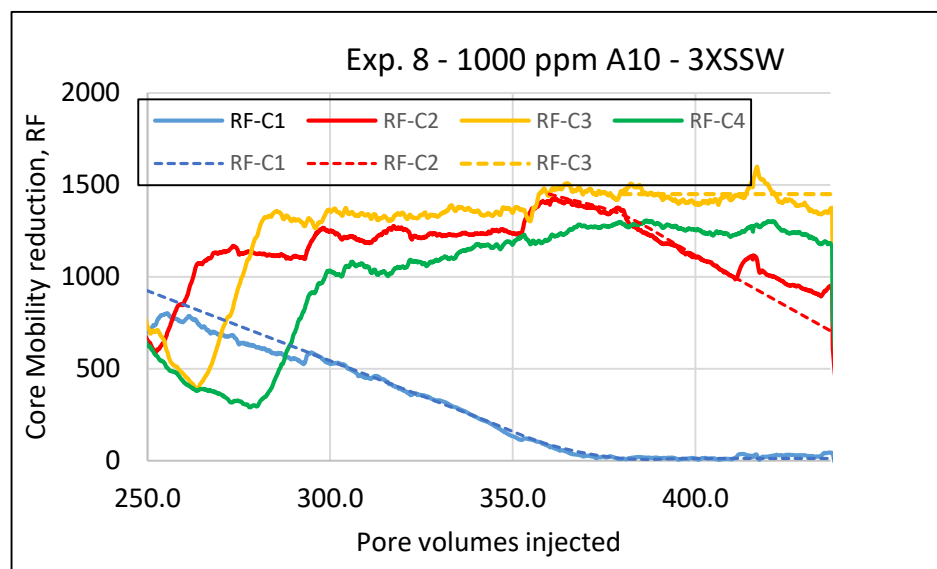Fig. 5.8 Mobility reduction at q =0.6 mL/min and varied temperature.

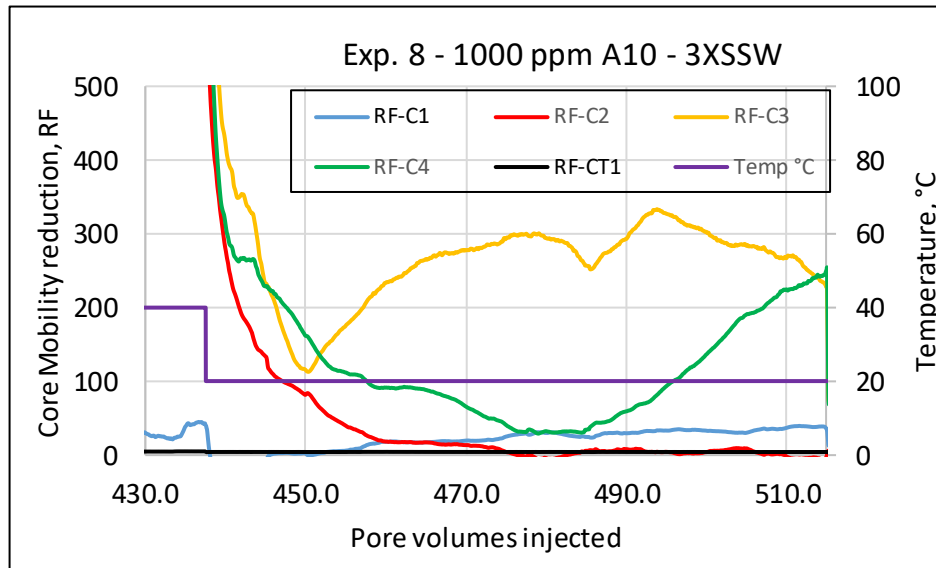

Fig. 5.9 Mobility reduction at q =0.6 mL/min at 40°C.

26

Fig. 5.10 Mobility reduction at q =0.6 mL/min at 20°C.

Fig. 5.10 shows the evolution in mobility reduction at 20°C; RF-C2 declined, followed by decline in RF-C3. The results in Fig. 5.10 support the Eq. 5.2 predictions. The decline in RF-C3, starting at pv = 494, was matched with $f = 0.013$, i.e., 2 times higher than at 40°C. From the prediction, RF-C4 would remain stable at approximately 300 for another 77 pv (=1/f) and thereafter start to decline.

Instead of further confirming this prediction, the polymer flow rate was increased to q = 3.0 ml/min and RF-C3 and RF-C4 declined, see Fig. 5.11. At pv = 543, we shifted to 3XSSW brine injection and the core segment mobility reductions decline further, see Fig. 5.12. The endpoint core permeability reductions, after injection of more than 287 pv of 3XSSW brine were 41,2, 5.7, 4.7 and 10.1, respectively. The relatively high front-core RRF may be explained by filtration – several hundred pv of polymer have been injected. Finally, we continued with injection of SSW brine and then distilled water. The endpoint permeability reductions are reported in Table 5.3.

Table 5.3 Endpoint permeability reduction.

Brine	Volume injected PV	RRF-C1	RRF-C2	RRF-C3	RRF-C4
3XSSW	287	41.2	5.7	4.7	10.1
SSW	374	85.2	11.3	1.2	1.6
DW	763	28.5	1.3	8.6	8.2

27
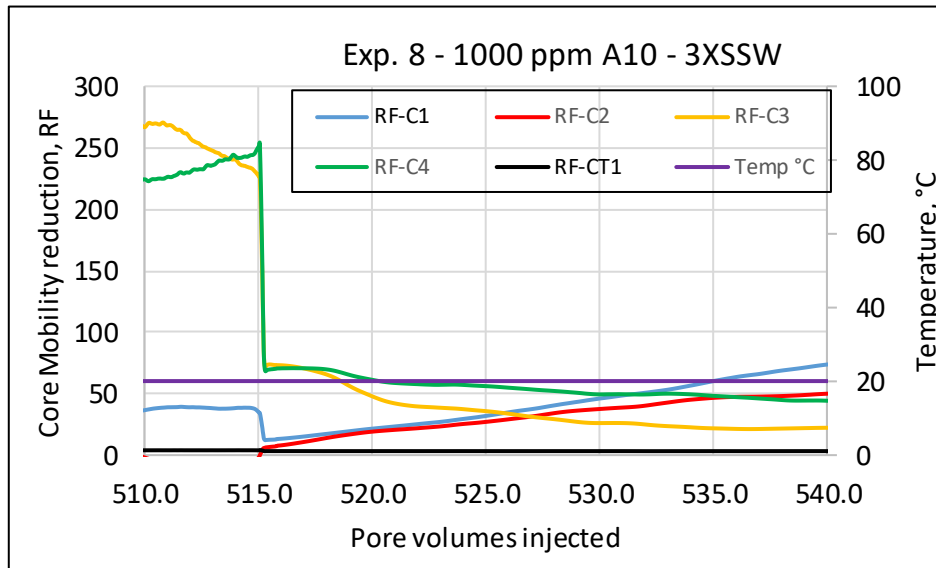
Fig. 5.11 Mobility reduction at q =3.0 mL/min at 20°C.
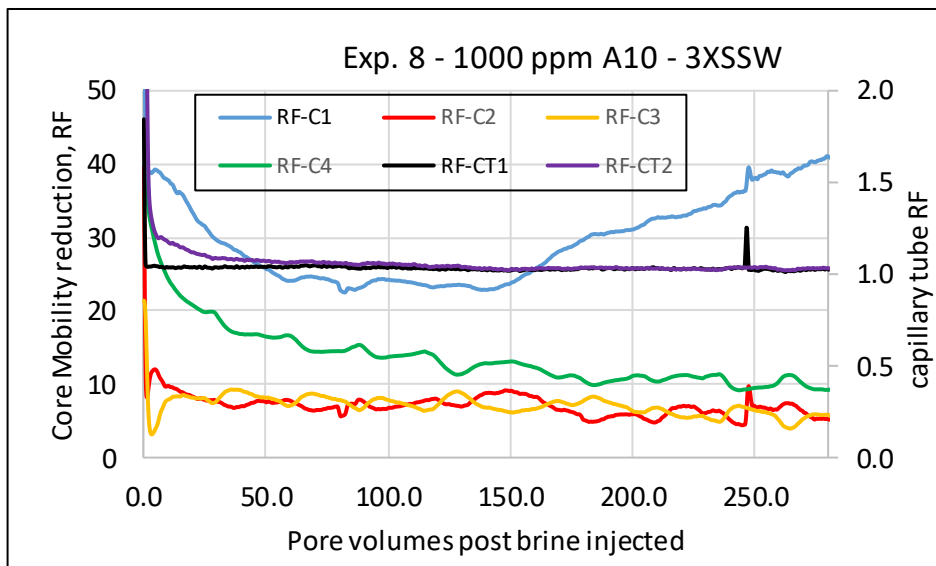
Fig. 5.12 Post brine mobility reduction at q =3.0 mL/min at 20°C.

Figs. 5.13 and 5.14 summarise the main findings from the 1000 ppm A10 polymer in 3XSSW brine. Fig. 5.13 shows the relative viscosity, i.e., capillary tube mobility reduction vs. temperature at the flow rates of 0.6 and 3.0 mL/min. The results may be interpreted as a weak thermo-thickening effect; the relative viscosity increased from 3.5 at 20°C to 5 at 80°C. The capillary tube ID = 1.01 mm (radius of 500 μm) and in terms of shear rate corresponds to 99 and 495 s^{-1}, respectively.

Capillary tube relative viscosity

● q = 0.6 ml/min   ● q = 3 ml/min

Fig. 5.13 Capillary tube mobility reduction vs. temperature.
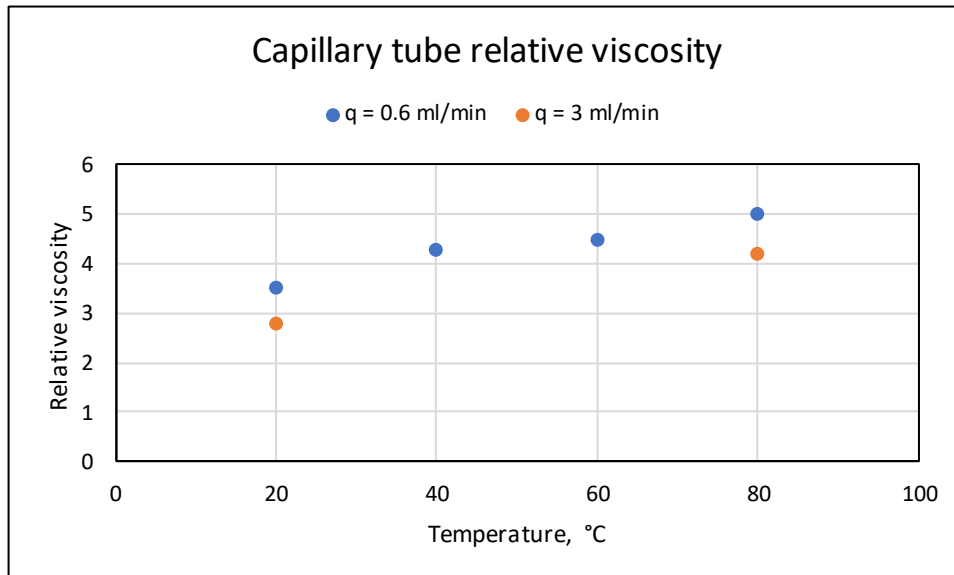
Core mobility reduction

● q = 0.6 ml/min   ● q = 3 ml/min
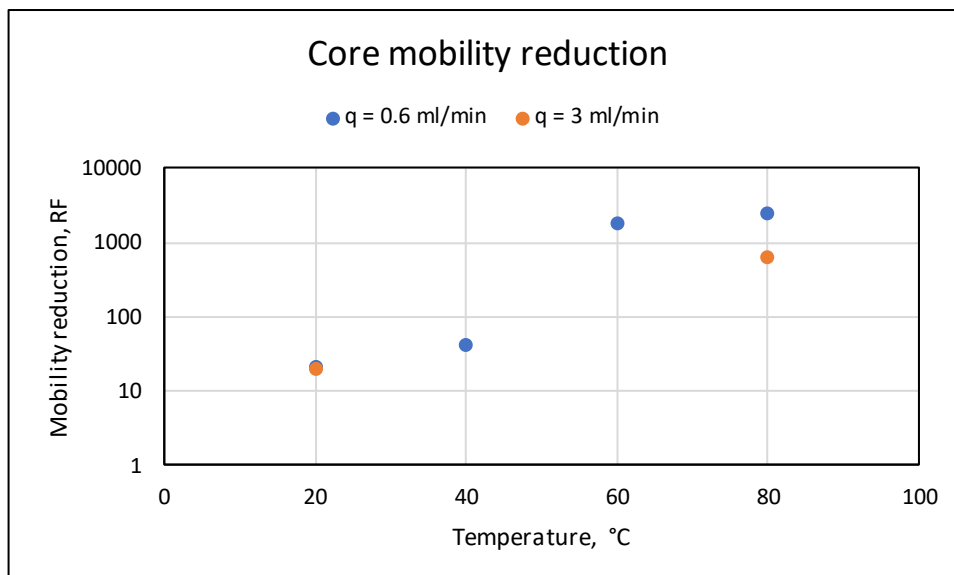
Fig. 5.14 Core mobility reduction vs. temperature.

Fig. 5.14 shows the corresponding core mobility reduction in the 11 Darcy sand column, with pore size of 16 μm. The following can be derived from the results in Fig. 5.14:

1. Significant thermo-thickening effect in porous media
2. At flow rate of 0.6 mL/min ($\dot{\gamma} = 8$ s^{-1}) core mobility reduction at 60°C and 80°C both exceed RF = 1000 and is three order of magnitude higher than the capillary tube mobility reduction
3. At flow rate of 0.6 mL/min ($\dot{\gamma} = 8$ s^{-1}) core mobility reduction at 40°C and 20°C are both less than RF = 50
4. Mobility reduction decreases by increasing the shear rate

If the polymer had been injected at stepwise increased temperature (as in the first experiments), we would, for this system, have observed the following: No thermo-thickening effect at 20 and 40°C and thermo-thickening effect at 60 and 80°C.

Whether, the difference in thermo-thickening is only a factor of scaling, pore size varied from 16 μm in the sand to 500 μm in the tube, or that thermo-thickening also depends on anchoring sites for adsorbed polymer is not fully understood. Previously we have argued on the need for anchoring sites to be able to achieve high mobility reduction. However, results from new experiments by narrowing down the capillary tube radius, combined with core flood experiments in ultra-high permeability sand may contribute with new information.

6 Conclusion

Thermo-thickening effect has been demonstrated for low MW ATBS-based associative polymers. In SSW brine the low associative content polymer, A06, was thermo-thickening at polymer concentration of 2700 ppm, but not at 1000 ppm.

By increasing the associative content, using A08 and A10 polymers, thermo-thickening was observed also at polymer concentration of 1000 ppm. The relative viscosity in capillary tube viscometer was 4 and the core mobility reduction at elevate temperature was 2 order of magnitude higher. The high core mobility reduction was induced by temperature; at 20°C the core mobility reduction was like a regular polymer.

In terms of core mobility reduction, core mobility reduction vs. shear rate was approximately the same in 1 D sandstone and 10 D sand.

It was however observed decline or collapse of pore blocking polymer network at low flow velocity. This effect seems to depend on the associative content. In-line viscosity in the 7-cm core measurements do not support any viscosity decay or polymer degradation.

When the 7-cm flood experiments were upscaled to 80-cm flood experiments using the 1000 ppm A10, thermo-thickening was observed in the first ¾ of the sand column. However, the mobility reduction declined along the length. A rerun using 3 times higher brine salinity revealed high and stable mobility reduction in all sections of the column.

7 References

Lohne, A., Stavland, A. and Reichenbach-Klinke, R. 2019. Modeling of Associative Polymer Flow in porous medium. Paper presented at the IOR 2019 – 20th European Symposium on Improved Oil Recovery, Pau, France, 8-11 April.

Reichenbach-Klinke, R., Zimmermann, T., Stavland, A., Berland, H. and Strand, D. 2017. Temperature-switchablePolymer forEnhanced Oil Recovery. Paper presented at the IOR 2017 – 19th European Symposium on Improved Oil Recovery, Stavanger, Norway, 24-27 April.

8 Appendix

8.1 Does porosity and permeability of sand depend on pressure?

When packing sand in columns, the porosity is normally constant and the variation in porosity is less than 1%. For sand packed in columns the bulk volume is fixed and there is no overburden pressure. When sand is packed into a core holder and the overburden pressure is increased the bulk volume is no longer fixed and the accuracy in porosity can be questioned. However, we know the matrix volume, $V_m = {}^m/_\rho$, i.e., the mass of added sand and we derive the pore volume, V_p.

$$\frac{V_m}{V_p} = \frac{1-\varphi}{\varphi} \qquad \text{Eq. 8.1.1}$$

The bulk volume, $V_b = {}^{V_p}/_\varphi$. If knowing the length of the sand-packed core we can derive the effective diameter.

Example, the porosity of sand packed into a column is $\varphi = 0.346$. The same sand packed into a rubber sleeve with 50 bar over burden pressure gave $\varphi = 0.326$. and the effective diameter was reduced by a factor of 1.04.

From Carman-Kozeny we have:

$$k = \frac{D_p^2 \varphi^3}{72\tau(1-\varphi)^2} \qquad \text{Eq. 8.1.2}$$

If particle size and tortuosity are not altered by pressure, the permeability ratio between a pressurized, k_p, and not-pressurized sand, k_{n-p}, is the following:

$$\frac{k_{n-p}}{k_p} = \left(\frac{\varphi_{n-p}}{\varphi_p}\right)^3 \left(\frac{1-\varphi_p}{1-\varphi_{n-p}}\right)^2 \qquad \text{Eq. 8.1.3}$$

In this case, $\varphi_{n-p} = 0.346$ and $\varphi_p = 0.326$ we get $\frac{k_{n-p}}{k_p} = 1.27$, i.e., the permeabiliy decreases by increasing the overburden pressure.

8.2 Polymer samples

Through the execution of the 76-cm long core flood experiments, 120 Liter of 1000 ppm polymer was prepared and injected. Batches of 1% mother solution were prepared and stored in fridge and on regular basis further diluted to 1000 ppm, each of approximately 5-liter. At the flow rate of 3 mL/min we refilled the reservoir daily. At flow rate of 0.6 mL/min,

we refilled every fourth or fifth day. In total, over the 2-month injection period, we refilled the reservoir 29 times. For each sample we measured the viscosity, as reported in Table 8.2.1. The viscosity was derived from an Anton Paar Physica rheometer, using cone and plate geometry at 20°C. The reported viscosity is the average viscosity at shear rates 5.65 to 0.94 s^{-1}. Viscosity vs. shear rate for a typical sample is shown in Fig. 8.2.1. As, seen, the viscosity is weakly shear thinning and can be matched with a Carreau-model.

The viscosity data reported in Table 8.2.1 are plotted in Fig. 8.2.2. There are some viscosity variations and we speculate on that part of this variation is because of the foam generation during N2-bubbling. However, some of the viscosity fluctuations were observed in the core mobility reductions, see Fig. 5.2. We clearly observe that the viscosity is higher in 3XSSW brine than in SSW brine.
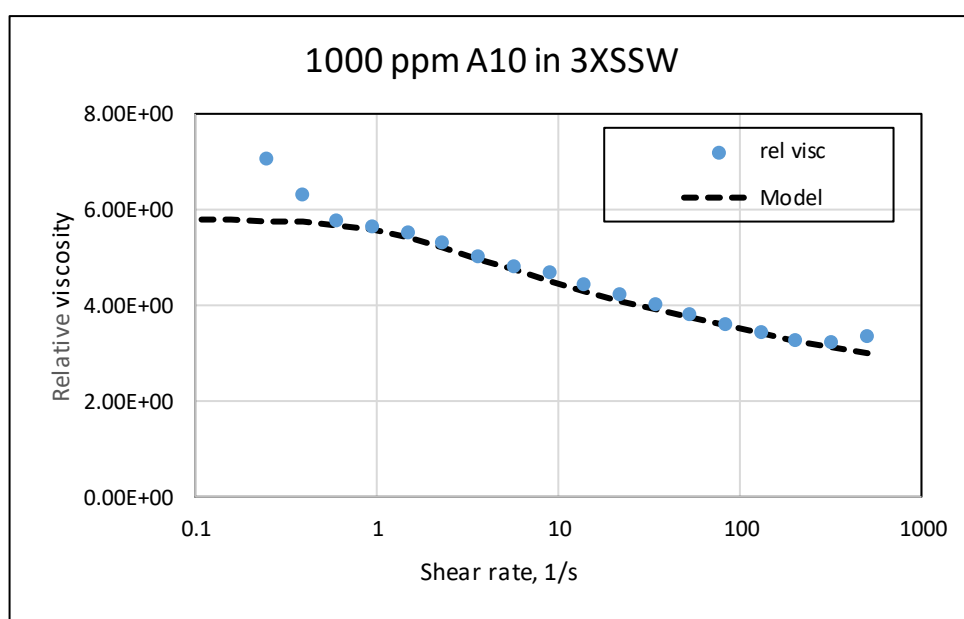

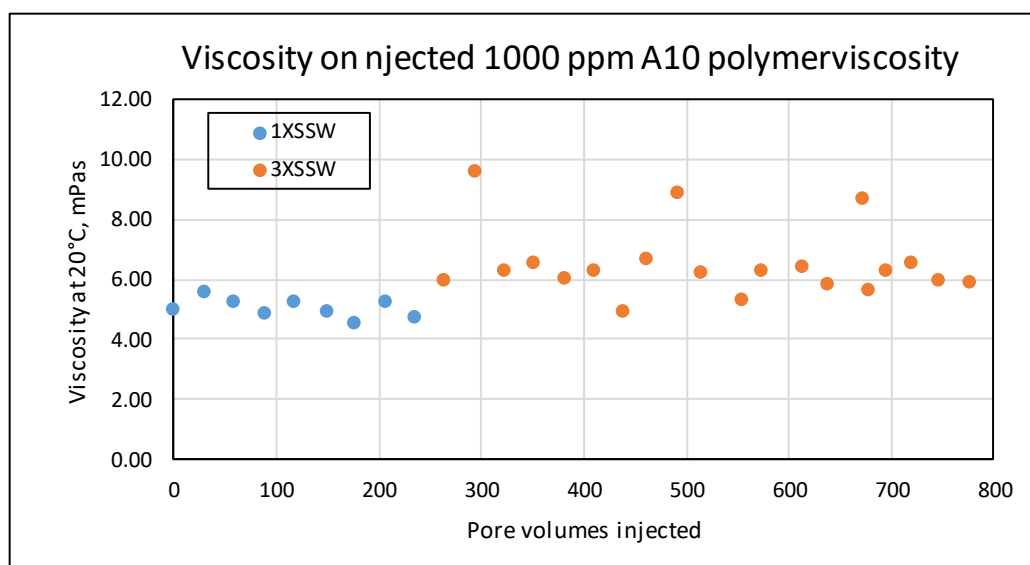Fig. 8.2.1 Relative viscosity for 1000 ppm A10 in 3XSSW at 20°C.

Fig. 8.2.2 Viscosity for 1000 ppm A10 samples, viscosity measured at 20°C.

Table 8.2.1 Prepared polymer samples.

Sample	Refill Time	PV	Visc, mPas
1	25.11.2019 13:36	0.0	5.03
2	26.11.2019 14:35	30.4	5.58
3	27.11.2019 14:00	58.8	5.23
4	28.11.2019 14:33	88.7	4.89
5	29.11.2019 13:46	116.9	5.24
6	30.11.2019 15:49	148.6	4.93
7	01.12.2019 14:09	175.7	4.54
8	02.12.2019 14:30	205.3	5.29
9	03.12.2019 15:06	235.2	4.74
10	04.12.2019 13:36	262.6	5.95
11	05.12.2019 14:30	292.8	9.58
12	06.12.2019 14:55	322.5	6.30
13	07.12.2019 13:57	350.5	6.57
14	08.12.2019 15:25	381.4	6.05
15	09.12.2019 14:30	409.5	6.28
16	10.12.2019 14:30	438.7	4.91
17	11.12.2019 14:15	461.6	6.70
18	16.12.2019 15:10	491.0	8.90
19	20.12.2019 14:10	514.0	6.26
20	27.12.2019 12:30	554.7	5.34
21	30.12.2019 14:35	572.7	6.27
22	06.01.2020 14:50	613.7	6.42
23	10.01.2020 15:25	637.2	5.86
24	16.01.2020 15:25	672.0	8.74
25	17.01.2020 14:47	677.9	5.64
26	20.01.2020 14:53	695.5	6.28
27	24.01.2020 14:53	718.8	6.54
28	29.01.2020 14:38	745.0	5.99
29	03.02.2020 14:37	777.2	5.93

NORCE Norwegian Research Centre AS
www.norceresearch.no